(2)

SECURITY CLASSIFICATION OF THIS PAGE

CUMENTATION PAGE

Form Approved
OMB No. 0704-0188

AD-A238 859

1b. RESTRICTIVE MARKINGS

2a

2b ...ION/DOWNGRADING SCHEDULE

3. DISTRIBUTION/AVAILABILITY OF REPORT
Approved for public release; distribution is unlimited

4. PERFORMING ORGANIZATION REPORT NUMBER(S)

5. MONITORING ORGANIZATION REPORT NUMBER(S)
AFOSR-TR- 91 0633

6a. NAME OF PERFORMING ORGANIZATION	6b. OFFICE SYMBOL (If applicable)	7a. NAME OF MONITORING ORGANIZATION
Dept of Aeronautics and Astronautics		AFOSR/NA

6c. ADDRESS (City, State, and ZIP Code)	7b. ADDRESS (City, State, and ZIP Code)
Cambridge, MA 02139	Building 410, Bolling AFB DC 20332-6448

8a. NAME OF FUNDING/SPONSORING ORGANIZATION	8b. OFFICE SYMBOL (If applicable)	9. PROCUREMENT INSTRUMENT IDENTIFICATION NUMBER
AFOSR/NA		AFOSR-86-0019

8c. ADDRESS (City, State, and ZIP Code)	10. SOURCE OF FUNDING NUMBERS			
	PROGRAM ELEMENT NO.	PROJECT NO.	TASK NO	WORK UNIT ACCESSION NO.
Building 410, Bolling AFB DC 20332-6448	61102F	2038	A1	

11. TITLE (Include Security Classification)
Non-Equilibrium and Radiation in MPD Plasmas

12. PERSONAL AUTHOR(S)

13a. TYPE OF REPORT	13b TIME COVERED	14. DATE OF REPORT (Year, Month, Day)	15. PAGE COUNT
Final	FROM 5/1/90 TO 1/31/91	May 31, 1991	21

16. SUPPLEMENTARY NOTATION

17. COSATI CODES			18. SUBJECT TERMS (Continue on reverse if necessary and identify by block number)
FIELD	GROUP	SUB-GROUP	Electric Propulsion, Plasma Non-equilibrium

19. ABSTRACT (Continue on reverse if necessary and identify by block number)

This Report discusses work on Grant AFOSR 86-0119 for the period 5/1/90-1/31/91. Previous work on ionization non-equilibrium is summarized, and new results pertaining to inlet ionization in MPD thrusters are presented. Brief summaries are also given of our work on transport effects, Hall effects magnetic layers and electrothermal arcjets.

91-05930

20. DISTRIBUTION/AVAILABILITY OF ABSTRACT	21. ABSTRACT SECURITY CLASSIFICATION
☒ UNCLASSIFIED/UNLIMITED ☒ SAME AS RPT ☐ DTIC USERS	Unclassified

22a. NAME OF RESPONSIBLE INDIVIDUAL	22b. TELEPHONE (Include Area Code)	22c. OFFICE SYMBOL
Dr. Mitat Birkan	202-767-4937	AFOSR/NA

DD Form 1473, JUN 86 — Previous editions are obsolete. — SECURITY CLASSIFICATION OF THIS PAGE

SPACE POWER AND PROPULSION LABORATORY

Department of Aero/Astro

MIT

Cambridge, Ma. 02139

Non-Equilibrium and Radiation in MPD Plasmas

Final Report for the Period 5/1/90 to 1/31/91

on Grant AFOSR 86-0119

Attention Dr. Mitat Birkan
AFOSR/NA
Bolling AFB
Washington, DC 20332

by

Manuel Martinez-Sanchez
MIT Dept. of Aeronautics and Astronautics

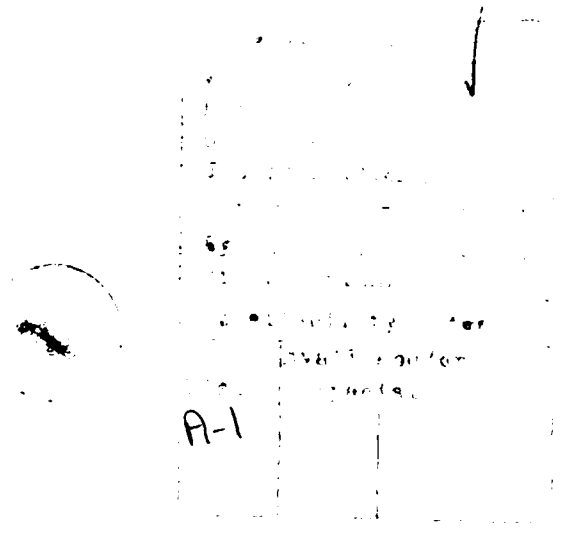

Abstract

This Report discusses work on Grant AFOSR 86-0119 for the period 5/1/90-1/31/91. Previous work on ionization non-equilibrium is summarized, and new results pertaining to inlet ionization in MPD thrusters are presented. Brief summaries are also given of our work on transport effects, Hall effects magnetic layers and electrothermal arcjets.

1. Introduction

This Final Report summarizes the results of our work on plasma non-equilibrium issues, under Grant AFOSR-86-0119. Results to 4/30/90 have been documented in our previous Annual Reports, so we will here concentrate on the final segment of the Grant covering the period 5/1/90-1/31/91.

The main responsibility for the work on Radiation and Non-equilibrium has been on doctoral candidate Eric Sheppard, who has been directly supported by the Grant. In addition the existence of AFOSR's Grant, and the resultant research activity, has attracted several other self-supporting students, who have also contributed significantly to our progress. These include doctoral candidates J. Marc Chanty, Eli Niewood and Scott Miller. Recently, the Air Force Phillips Lab. has entered into a cooperative program with us, and a doctoral student, Mr Eric Gaidos, will be starting experimental MPD work at Edwards AFB this Summer. Also recently initiated is arcjet modeling work by a new Master's student, Miss A. Sakamoto.

The object of our research has been the basic physics of plasma thrusters, particularly MPD thrusters. More specifically, within the context of the present Grant, we have addressed the complex of issues which encompass excitation - ionization kinetics of MPD plasmas, and their effects on thruster flows.

The work on the detailed kinetics of electronic excitation of Argon and Hydrogen was summarized in the paper by E. Sheppard and M. Martinez-Sanchez (AIAA 90-2608) which is appended to this Report. Because of their intimate coupl ing, excitation, line radiation and ionization effects must be considered together. The situation in MPD thrusters (as opposed to arcjets) is far from Local Thermodynamic Equilibium (LTE), and modeling has to be based on a detailed set of atomic level population balances. We included three basic non-equilibrium drivers.

(a) Radiation escape. The majority of the spectrum is optically thin (with the exception of the central regions of resonant lines), and there is therefore a continuous net radiative depopulation rate of all excited states.

(b) Diffusion. Due to the prevailing low density, MPD plasmas share many to the characteristics of glow discharges, including the prevalence of ambipolar diffusion as a loss mechanism for ion-electron pairs. This requires continuous excess ionization to maintain the ionic balance, and this cascades down the excited level populations.

(c) Dynamic Lag. Any given parcel of plasma flowing through a thruster experiences rapidly changing background conditions and many of its internal degrees of freedom lag widely behind shifting equilibrium. This is most extreme at the channel inlet, where gas goes in a few microseconds from room conditions to over an eV background energy. Overall ionization equilibrium (Saha's law) is clearly violated. Other processes, such as population/depopulation level kinetics remain close to balanced in a quasi-static sense.

Using multi-level models with the quasi-static approximation for internal balancing, we derived expressions and values for line radiation density, non-Boltzmann population distributions and overall ionization-recombination rate coefficients. It was found that radiative loss can account for at most a few percent of the input power to an MPD thruster, in good agreement with experimental (bolometer) data from the related field of coaxial plasma guns [1]. It was also found that care must be exercised when using the upper level populations of excited Argon ions for T_e measurements, since significant deviations occur from the normally assumed equilibration with the free electrons. This is not, however, the case with neutral Argon, although, unfortunately, its lines are normally much weaker.

2. Inlet Ionization Effects

The inlet relaxation problem has been one of the most important and difficult areas of uncertainty in plasma devices, Non-equilibrium MHD generators suffer global instabilities due to this problem[2]. Our own experimental MPD thruster[3] failed to produce an azimuthally uniform discharge when the inlet electric field was too weak due to a convergent-type design. Japanese experiments[4] showed that Hydrogen would ionize very weakly and with large delays in a thruster in which Argon showed no such difficulties. The gas enters these devices with no ions or free electrons, and a rapid process of electron multiplication must take place, starting with a few back-diffused or photoionized electrons. As the case of Hydrogen vs. Argon shows, the details of the kinetics of intermediate"radicals" can control the whole process, in analogy with the ignition delay problems in high speed combustors.

One type of injector which is potentially important for steady-state MPD thrusters is a ceramic porous plate (Fig. 1a). This is one limiting configuration which can be analyzed as a one-dimensional structure. In previous work, we have studied the dynamics of such an inlet layer assuming full ionization. We are now extending this by including kinetic equations for ionization and species diffusion. Radiation and excitation kinetics may also play a role, and will be assessed later.

A more common configuration involves discrete injector holes (Fig. 1B). Here, the diffusion of electrons into the fresh gas is mainly across streamlines, rather than against the flow, and the structure resembles a 3-D diffusion flame. The study in the three dimensional case is very difficult, and we will attempt to simplify it by using its slenderness to treat it as a submerged reacting jet. No results have yet been obtained for this configuration.

In either case, the results should indicate the length of the inlet relaxation zone, and also the threshold conditions below which no plasma ignition occurs. Both of these items are important design information for plasma devices.

Significant results have been obtained for the one-dimensional case. Because of the presence of the insulating (hence electron-repelling) back plate, the electron heat flux must be small in the ionization layer, and hence a constant T_e approximation is made. Assuming also a constant flow speed through the layer (an assumption to be removed later), one can integrate the

(a) Porous-Plug Injector

1-D model of ionizing front:

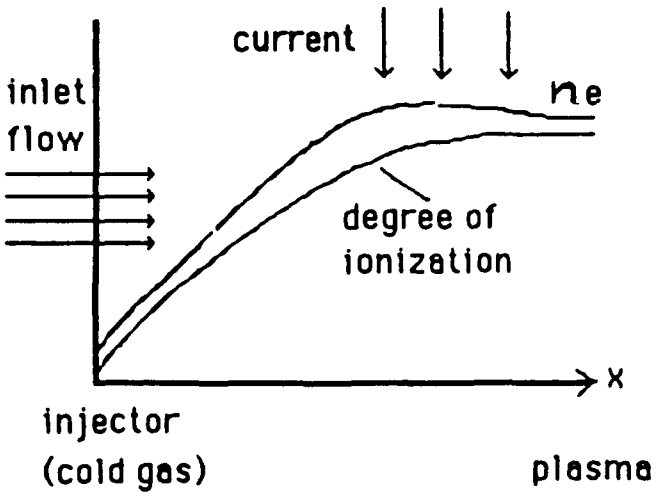

Fig. 1(a). Schematic variation of plasma quantities near a 1-D (porous plug) injector.

Questions:

* What processes control?
* How thick is the front?
* Under what conditions is there a solution? (ignition conditions)

(b) Individual Injector Jet

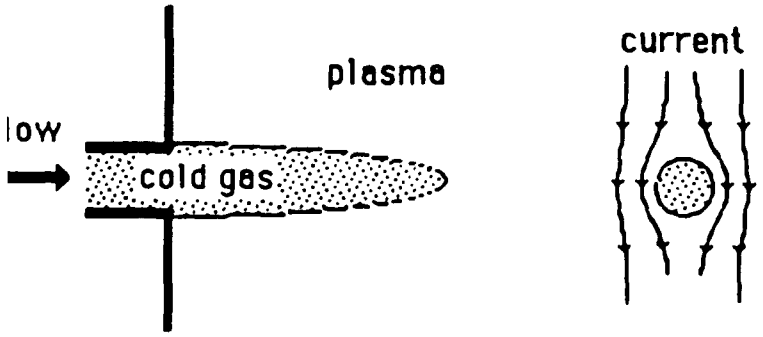

Fig. 1(b). The flow field around an individual injector jet.

Questions:

* How does background plasma interact with the fresh cold gas?
* How long is the "jet"?
* How does the "jet" interact with the Lorentz forces?

Argon Ionization Distance and Maximum Inlet Speed

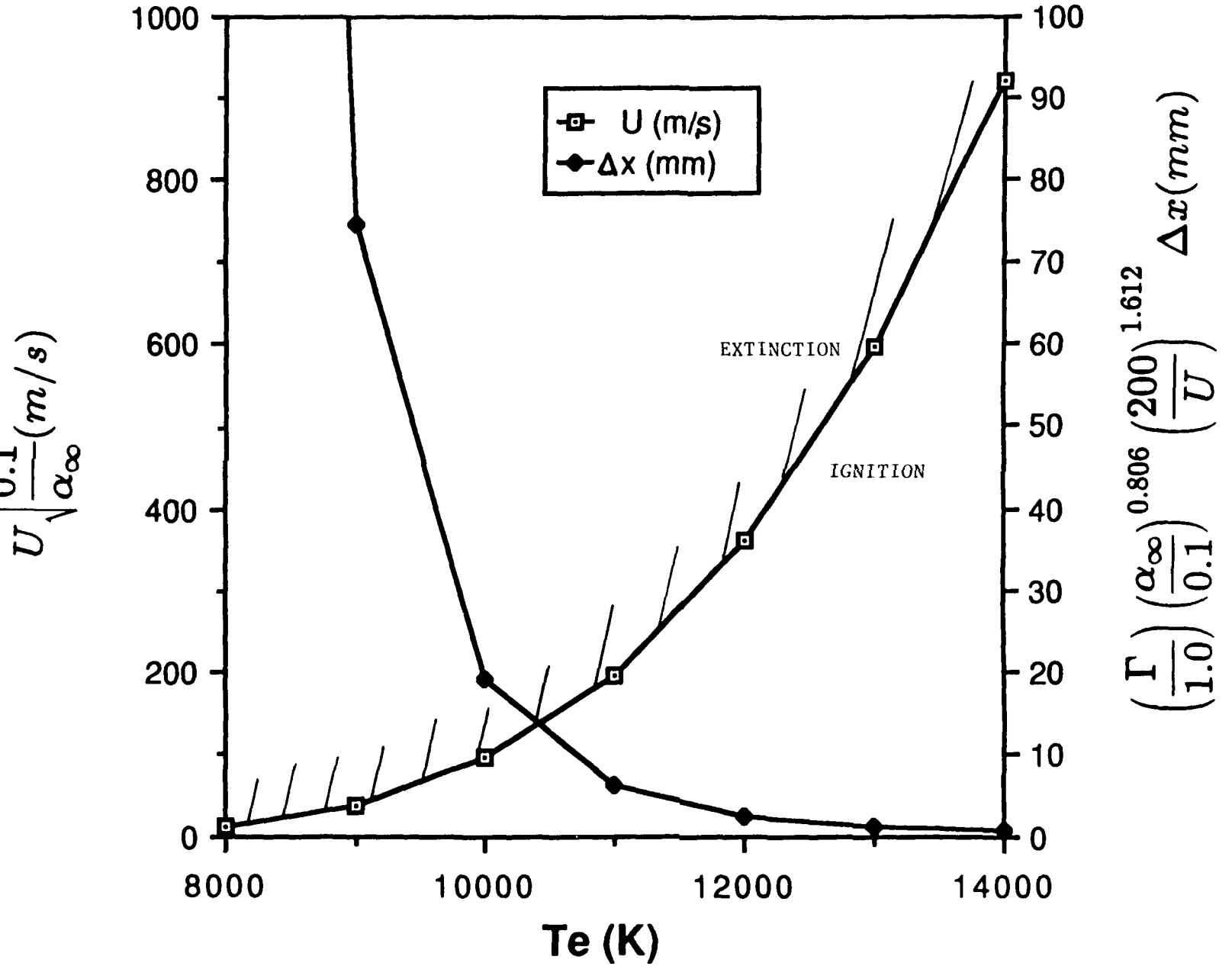

Fig. 2

concection-diffusion - ionization equations between a wall condition relating diffusive ion flux to Bohm velocity times local density and and a downstream asymptotic plasma state. It is found that no attached ionization layer can exit beyond a flow velocity (which increases strongly with electron temperature). When an attached ionization layer does exist, its thickness varies as $(\text{velocity})^{0.6}$ and decreases exponentially with T_e. For $T_e \geq 1$ eV and reasonable conditions, in Argon, the layer thickness is found to be a few mm. or less. The near-back plate electron density is found to be high enough to support strong electron thermal conductivity, hence validating the $T_e \cong$ constant assumption. These results are summarized in Fig. 2.

The above model concentrated on the counteracting effects of convection and diffusion, and ignored the flow dynamics. At the opposite extreme, our earlier models[5] studied the flow dynamics in the acceleration region while ignoring ionization effects.

In reality, plasma acceleration occurs simultaneously with the Ohmic dissipation which feeds ionization, and both effects should be considered together. Retaining the constant-temperature approximation, ignoring bulk recombination, lateral diffusion and area variation in the ionization-accerleration layer, the governing equations are

$$(n_e + n_n)\, u = G \tag{1}$$

$$m_i\, G\, u + n_e\, k\, (T_e + T_g) + n_n\, k\, T_g + \frac{B^2}{2\mu_o} = F \tag{2}$$

$$\frac{d}{dx}\left(n_e\, u - D_a \frac{dn_e}{dx}\right) = R\, S\, n_n\, n_e \tag{3}$$

$$e\, V_i\, R\, S\, n_n\, n_e = \sigma\, (E - u\, B)^2 \tag{4}$$

$$\frac{dB}{dx} = -\mu_o\, \sigma\, (E - u\, B) \tag{5}$$

where n_e, n_n are the electron-ion and the neutral density, respectively, $m_i G$ is the known mass flux, F is the (unknown) momentum flux, and separate electron and heavy species temperatures (T_e, T_g) are assumed, both taken as constants.

In Eq. (3), D_a is the ambipolar diffusion coefficient ($D_a\,(n_e + n_n) \cong$ const.), $R(T_e)$ is a Saha factor, such that RS is the ionization rate constant at the prevailing T_e. This T_e is to be inferred from the simplified electron energy balance in Eq. (4). Since $S(T_e)$ is an exponential function of T_e, small variations are to be expected, and a mean value suffices for non-sensitive functions of T_e. The one sensitive term is the right hand side of Eq. (3), where the whole source term is to be substituted from (4). Finally, in Eq. (5) the conductivity σ is assumed to be constant throughout, since, as will be seen, electron diffusion can maintain ionization fractions of over $\approx 1\%$ right down to the edge of the electron-repelling sheath on the injector plate.

Reorganizing Eqs. (3) and (5), they can be simultaneously solved for a set of three first derivatives such as $\frac{dn_e}{dx}$, $\frac{dB}{dx}$ and $\frac{d\Gamma_D}{dx}$, where $\Gamma_D \equiv D_a \frac{dn_e}{dx}$ is the backwards diffusive flux. when this is done, it is found that the set of differential equations has a singularity at

$$u = u^* = \sqrt{\frac{kT_i}{m_i}} \qquad (6)$$

Local analysis then shows that the singularity is of the repelling node type, such that no smooth crossing through the velocity u^* is possible within the region described by the given equations. Either the flow enters this region supercritically ($u > u^*$) or, at least, critically ($u = u^*$). For Argon at a few thousand degrees Kelvin, u^* is a few hundreds of m/sec. How the flow can reach the entrance speed is related to the constant-temperature assumption introduced, which implies a steady supply of thermal energy by conduction from regions downstream. This can provide the energy needed to "thermally choke" the arriving neutral gas flow.

Thus, the condition $u = u^*$ is a natural specification at $x = o$, together with $B = B_O$. Another one states that the total flux of ions at the sheath edge must be backwards, and must equal the sheath-entering Bohm flow:

$$\left(n_e u - D_a \frac{dn_e}{dx}\right)_{x=o} = - n_{e_o} v_B \qquad ; \; v_B = \sqrt{\frac{(kT_e + T_g)}{m_i}} \qquad (7)$$

Finally, at the downstream end we simply assume a length much greater than the ionization-acceleration distance, such that an asymptotic condition of zero current and zero gradients be reached [5].

This implies

$$\frac{du}{dx} = \frac{dn_e}{dx} = \frac{dB}{dx} = \frac{d\Gamma_D}{dx} = o \quad (x \to \infty) \qquad (8)$$

which, from Eq. (5) requires

$$u_\infty B_\infty = E \qquad (9)$$

The transverse electric field E is here arbitrary (within limits). Since the channel is thought of as possessing a throat somewhere downstream, different choices of E will dictate different area ratios A^*/A_O between throat and inlet. The largest choice of E is that for which $A^*/A_O = 1$, and smaller E values correspond to $A^*/A_O < 1$.

For numerical integration, the behavior at large x is important. An asymptotic analysis shows that, when the equations are linearized for conditions near u_∞, B_∞, etc, two characteristic modes occur, of which one diverges violently in the downstream direction, while the other converges at a

moderate rate. It is therefore necessary to integrate backwards. The procedure is roughly as follows: a set of values n_{e_∞}, B_∞ is guessed at. This plus the conditions at infinity, gives sufficient information to calculate analytically the amplitude of the acceptable downstream mode, and therefore to "step out" of the asymptotic limit by some small amount. From there, numerical integration is continued back to the inlet condition $B = B_0$. At this point the conditions $u = u^*$ and (flux = - Bohm flux) are checked, and iteration on B_∞, n_{e_∞} follows until they are both met.

Results for a case with convergence ratio $H^*/H_0 = 0.728$ and with a slightly supercritical inlet velocity are shown in Figs. 3 and 4a-4d. Several dimensionless parameters need to be defined for interpretation:

$$\lambda = \frac{u_{ref}}{u_{CIV}} \qquad \left(u_{ref} = \frac{B_o^2}{2\mu_o m_i G} \;, \; u_{CIV} = \sqrt{\frac{2V_i}{m_i}} \right) \tag{10}$$

$$\theta = \frac{T_i}{T_e + T_i} \tag{11}$$

$$\varepsilon_D = \frac{\sigma B_o^2}{2 m_i G^2} D_a \, (n_e + n_n) \tag{12}$$

$$p = \left(\frac{v_B}{u_{ref}} \right)^2 \tag{13}$$

of these, λ measures the more familiar (current)^2/(mass flow parameter, and should be of order 1 for operation near "onset" ($\lambda = 1$ taken for our example). θ must be small near the inlet, and we use $\theta = 0.1$ here. Similarly, ε_D measures the ratio of ambipolar to magnetic diffusivity (at the characteristic MPD density), and is a small parameter (0.1 used here). Finally, p is a measure of the gas pressure divided by Magnetic pressure, and the value $p = 0.05$ has been assumed.

Fig. 3 shows the normalized magnetic field $B' = B/B_0$ versus normalized distance

$$x' = \sigma \mu_o u_{ref} x \tag{14}$$

which can be interpreted as the Magnetic Reynolds number for a distance equal to x. B' is taken to decrease from 1 to 0.9, corresponding to the prescribed inlet velocity. The characteristic distance for B variation, namely, for the initial current concentration, is seen to be of the order $\Delta x' \approx 1$. This is found, within a factor of 2, for all conditions locked at so far, and is basically the same result obtained in Ref. 5 for frozen flow.

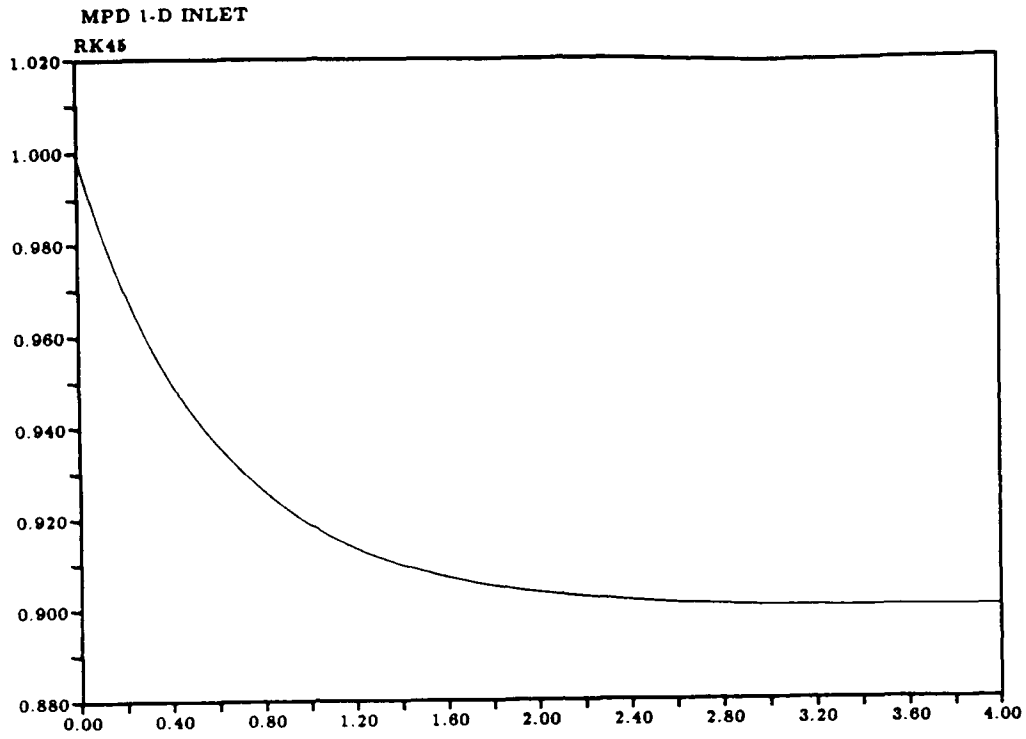
MPD 1-D INLET
RK45
1.020
1.000
0.980
0.960
0.940
0.920
0.900
0.880
0.00
0.40
0.80
1.20
1.60
2.00
2.40
2.80
3.20
3.60
4.00
B'
x'

Fig 3

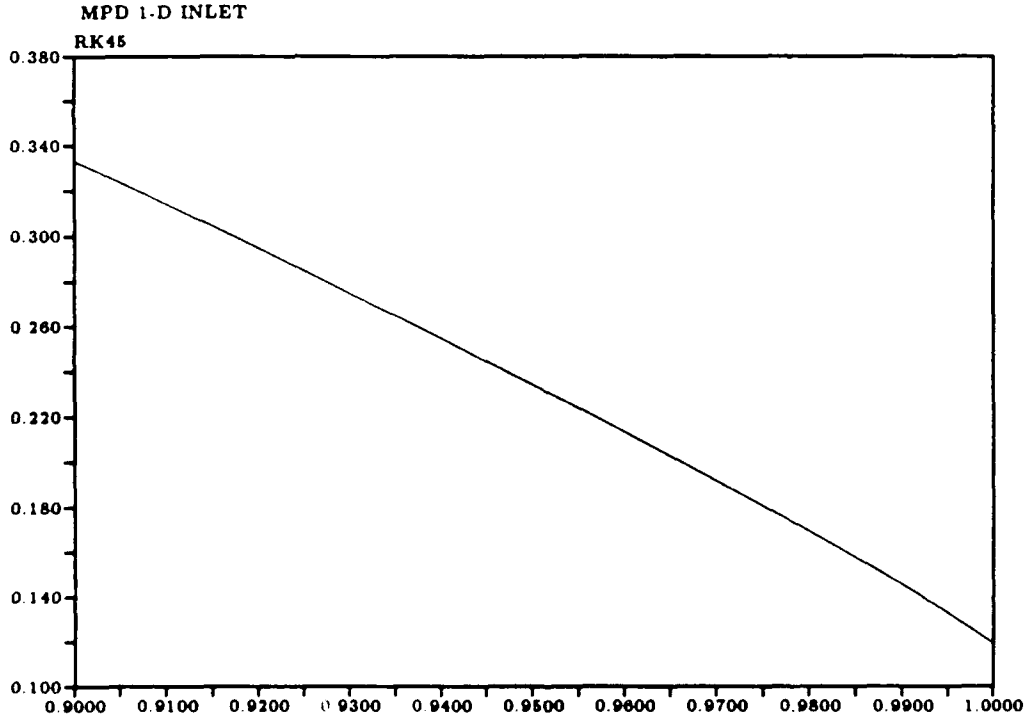
MPD 1-D INLET
RK45
0.380
0.340
0.300
0.260
0.220
0.180
0.140
0.100
0.9000
0.9100
0.9200
0.9300
0.9400
0.9500
0.9600
0.9700
0.9800
0.9900
1.0000
u'
B'

Fig 4a

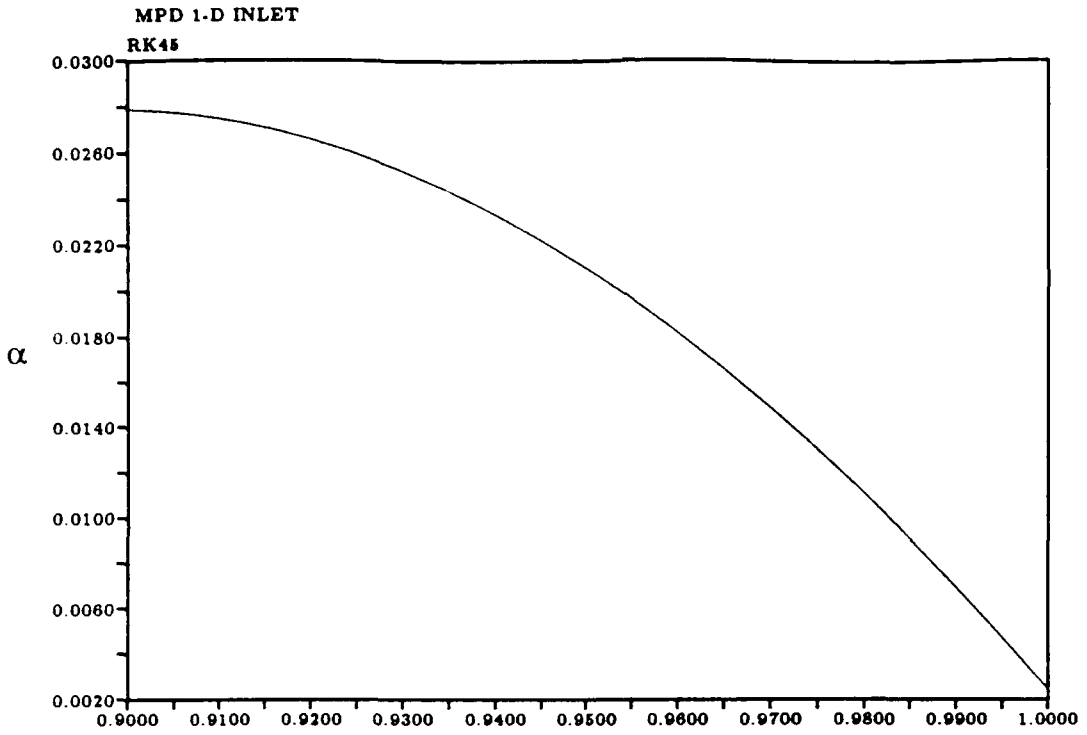

Fig. 4b B'

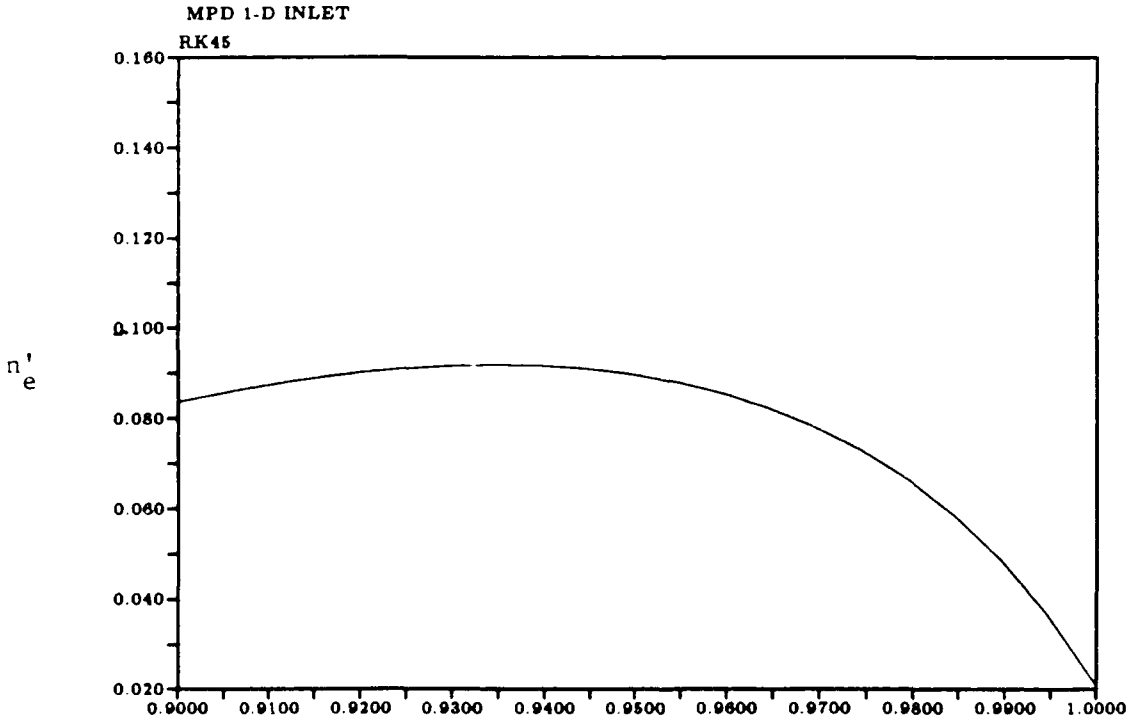

Fig. 4c B'

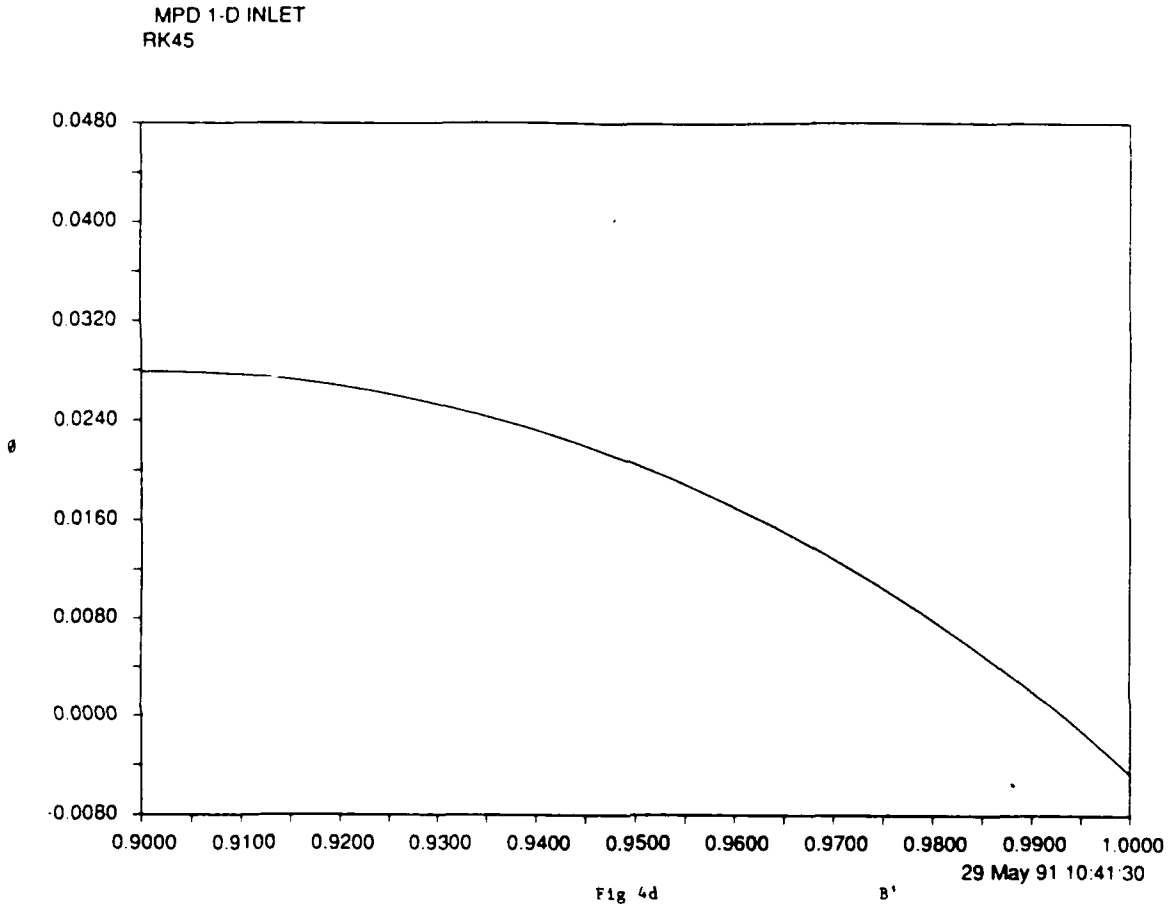
MPD 1-D INLET
RK45
0.0480
0.0400
0.0320
0.0240
0.0160
0.0080
0.0000
-0.0080
ø
0.9000
0.9100
0.9200
0.9300
0.9400
0.9500
0.9600
0.9700
0.9800
0.9900
1.0000
29 May 91 10:41:30

Fig 4d B'

Fig. 4a shows the dimensionless velocity $u' = u/u_{ref}$ versus magnetic field B'. Here, u' increases from the slightly supercritical value of 0.1 ($u'^* = 0.0707$ in this case) to $u'_\infty = 0.333$, corresponding to $u_\infty = E/B_\infty$. Notice the nearly linear variation.

Fig. 4b gives the ionization fraction α vs. B'. The wall value $\alpha_o \cong 0.024$ results from satisfaction of the boundary condition of Eq. (7), and, as noted, is sufficiently high to assume a nearly constant (Coulomb dominated) conductivity throughout. The ionization fraction increased monotonically on approximately the same length scale as u'. This is because ionization is driven by dissipation (j^2/σ), while u' is driven by Lorentz force (jB), both of which concentrate in the same region.

The normalized electron density

$$n'_e = \frac{B_o^2}{2\mu_o m_i G^2}\, n_e \qquad (15)$$

is shown in Fig. 4c. The intermediate maximum is characteristic of other cases treated as well, and is due to the counteracting effects of continuing ionization on one hand, versus overall plasma expansion on the other.

Finally, Fig. 4d shows the normalized net ion flux

$$\phi = \frac{1}{G}\left(n_e u - D_a \frac{dn_e}{dx}\right) \qquad (16)$$

versus B'. Notice the negative inlet (B' = 1) value of ϕ, in consistence with Eq. (7)

So far, no value of T_e has been assumed. As noted, the appropriate T_e is dictated by Eq. (4), which contains the specific recombination rate function $R(T_e)$. Work is in progress now to asses the effect of using conventional models, such as the Hinnov - Hirschberg equation, versus our more detailed rate formulation of Paper AIAA 90-2608, on the obtained electron temperature.

3. Other Activities

3.1 Transport Effects in MPD. Scott Miller has completed development of a 2-D code which accounts for the full effect of viscosity, electron and heavy particles heat transfer and diffusion, while, at the same time fully coupling to the electromagnetic fields. This extends the work reported in the paper AIAA 90-2606, in which the magnetic field distribution was independently prescribed. Results for a channel with 2 cm. interelectrode separation, 10 cm active length, with $\dot{m}$(Argon) = 4 g/sec and I = 35 KA are shown in Fig. 5. The

Two-Dimensional Viscous MPD Flow

Magnetic Field

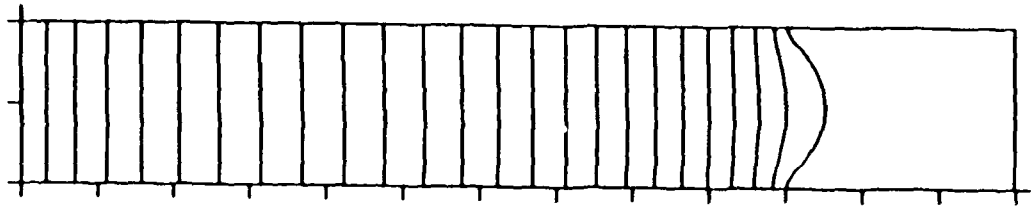

Max = 0.1T
Min = 0.0T
Inc = 0.004T

Fluid Velocity

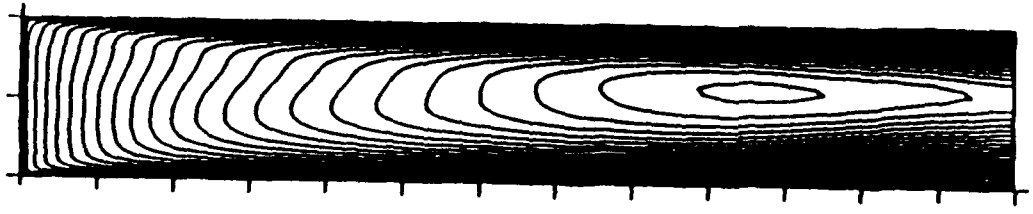

Max = 5000m/s
Min = 0 m/s
Inc = 200m/s

Fig. 5

Gas Temperature

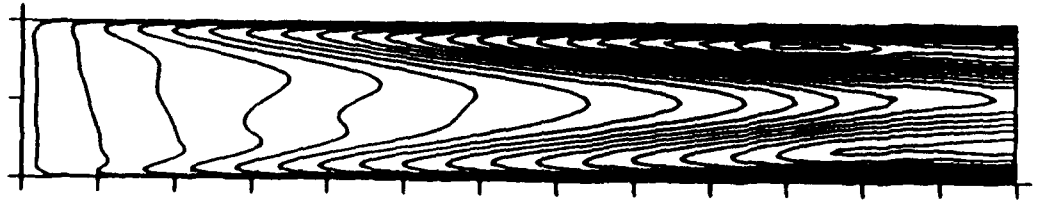

Max=10000K
Min = 0K
Inc = 400K

first panel shows the current lines to be only slightly convected/distorted, which is a result of ignoring the Hall effect. The velocity distribution shows boundary layers which nearly reach full development at exit, and which create substantial drag forces. Finally, the gas temperature shows the classical hypersonic boundary layer overshoots, peaking at about 1 eV near the channel exit. The lack of symmetry in the temperature and velocity maps is due to the effects of heat transport and expansion work of the electron gas as it drifts transversely.

3.2 The Hall Effect and its Consequences

While the solutions just discussed incorporated many real gas effects, they still ignored anisotropic electron conductivity. Eli Niewood has been working on the inclusion of this important effect, which presents great numerical difficulties due to the steepness of the gradients it induces. By gradually refining the formulation, particularly at and near the electrode boundaries, the latest results already meet all the conservation tests to reasonable accuracy. In these calculations, heat transport was included, as well as ambipolar diffusion, but viscosity was not. For the same case as that of Fig. 5, the results are shown in Fig. 6. The current lines are now drastically distorted, especially near the anode (lower electrode). The Hall effect causes the current lines to enter the anode at an angle $\tan^{-1}\beta$ ($\beta = \frac{\sigma}{en_e} B$ is the Hall parameter), which becomes large at low electron density. Simultaneously, the Lorentz $\vec{j} \times \vec{B}$ force pushes the plasma in a direction perpendicular to the current vector, which near the anode points mainly away from the electrode surface, and creates a hydrostatic pressure gradient with a deep minimum at the surface. Thus, these two effects reinforce each other, and are eventually checked only by diffusive and ohmic damping. The result is the creation of a largely depleted thin layer where β can reach values of the order of 10-20, while β remains of order 1 in the bulk. In a uniform plasma, $\beta \geq 2-3$ would be expected to create an ionization instability [6], but the large gradients and the immediately adjacent wall serve to prevent its development in this case (although, in a sense, the very formation of the depleted layer may be thought of as the final stage of this type of instability).

From a practical standpoint, the essential consequence of this effect is the creation of a large anode voltage drop. This is because of the Hall component of Ohm's law:

Two Dimensional MPD with Hall Effect

Current Lines

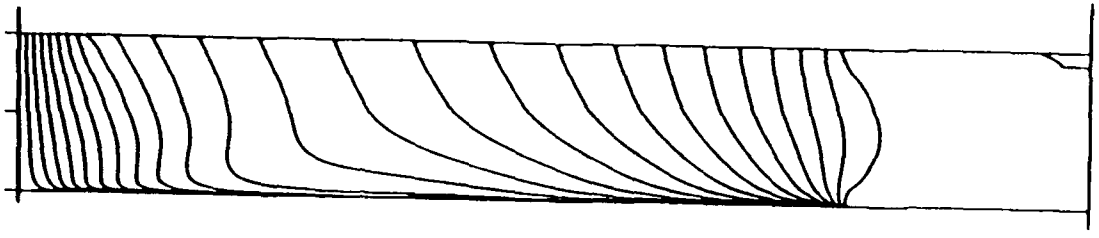

Max = 0.1 T
Min = 0.0 T
Inc = 0.002 T

Electron Temperature

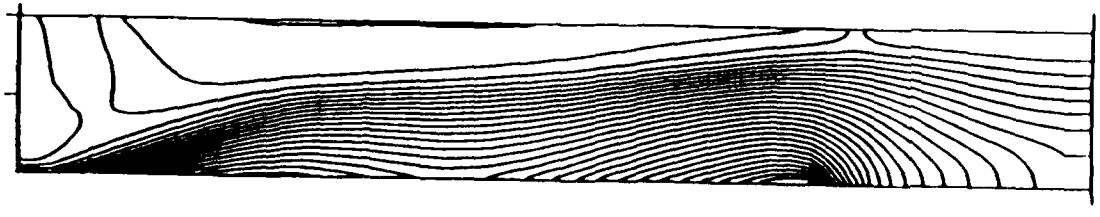

Max = 34000 K
Min = 10000 K
Inc = 500 K

Fig. 6

Ionization Fraction

Max = 1.0
Min = 0.0
Inc = 0.02

$$\sigma\left(\vec{E} + \vec{u} \times \vec{B} + \frac{kT_e}{en_e} \nabla n_e\right) = \vec{j} + \vec{j} \times \vec{\beta} \qquad (17)$$

The density gradient term can itself be hydrostatically related to the Lorenz cross force. At full ionization (which, as shown by the second panel in Fig. 6 does occur near the anode), we have

$$kT_e \frac{\partial n_e}{\partial y} = j_x B \qquad (18)$$

and then the Y - component of (17) becomes

$$E_y = u B + \frac{j_y}{\sigma} - 2\frac{\beta}{\sigma} j_x \qquad (19)$$

and, since the X component of the left hand side of Eq. (17) is near zero at the wall, $j_x = -\beta j_y$, giving

$$E_y = u B + \frac{1 + 2\beta^2}{\sigma} j_y \qquad (20)$$

Since β is very large in the thin depleted layer, integration of Eq. (20) gives a large concentrated voltage drop occurring over distances of the order of one mm. This is illustrated in Fig. 7, which shows a transverse profile in the vicinity of the current peak of Fig. 6. Here, $\Delta V_a \cong 17$ Volts in the first mm., while the overall anode-cathode voltage is only 25 Volts. Incidentally, this ΔV_a matches well with that measured under almost identical conditions in our experiments on the joint MIT - R&D program [7,8].

It is appropriate to remark that, to our knowledge, this is the first satisfactory explanation ever reported for the anomalous anode drops occurring in MPD thrusters at high currents. Previous speculation had centered on sheath effects, perhaps complicated by magnetic effects. Our results indicate clearly a Hall origin for these drops, which occur in the quasineutral region of the plasma. This clarification may in time open ways to avoid such effects.

3.3 Magnetic Boundary Layers

The idealization in which the Ohmic component of the electric field is neglected when compared to the back emf is very useful for understanding the dynamics of bulk plasma, but fails in regions where the presence of specific boundary conditions impose the existence of localized current concentrations. A prototype of this behavior is the inlet (and to some extent

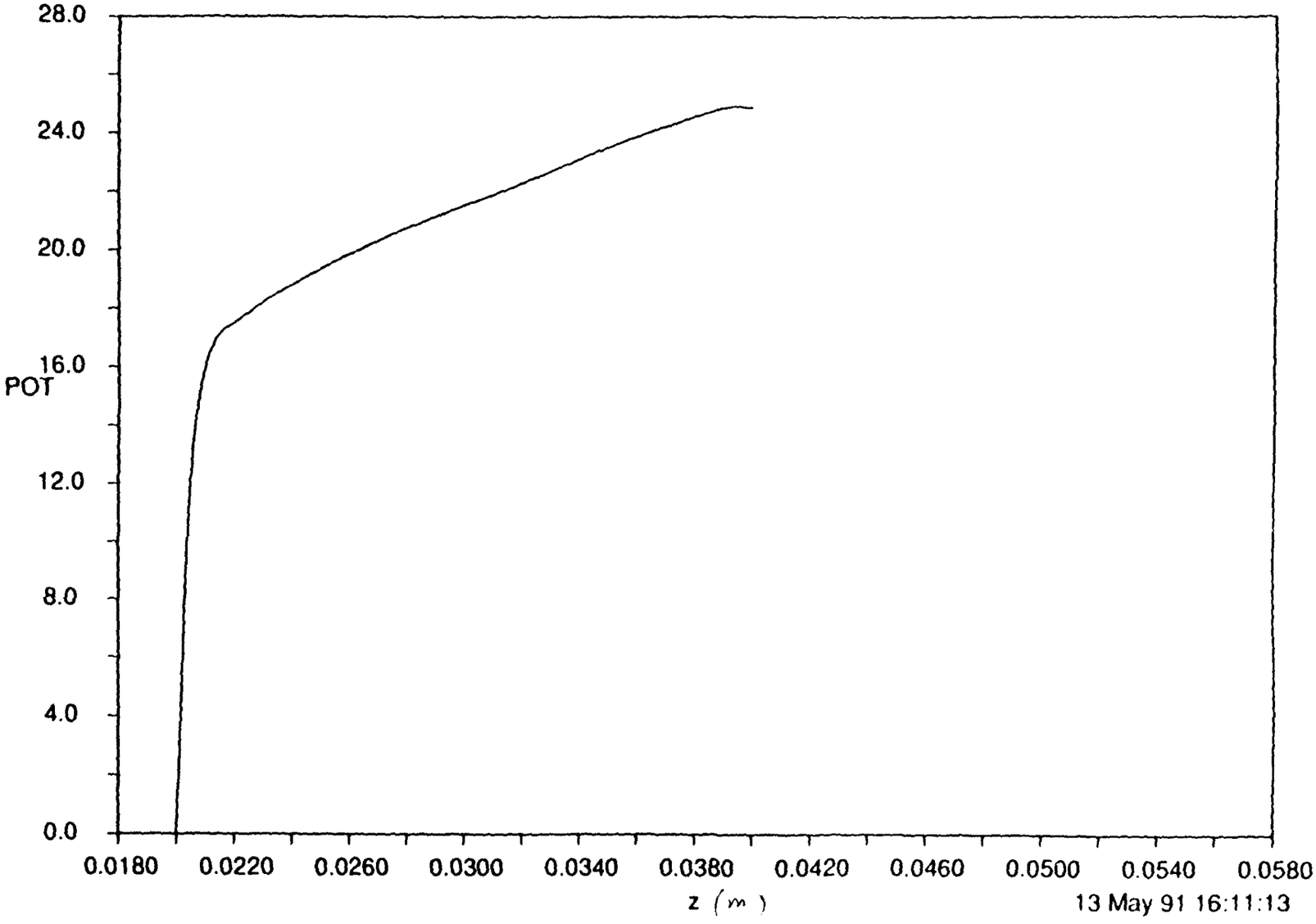
28.0
24.0
20.0
16.0
POT
12.0
8.0
4.0
0.0
0.0180
0.0220
0.0260
0.0300
0.0340
0.0380
0.0420
0.0460
0.0500
0.0540
0.0580
z (m)
13 May 91 16:11:13

Fig. 7

the exit) current concentrations in one-dimensional accelerators, treated in Ref. 5. J. Marc Chanty has developed the theory of these "magnetic layers" for several additional situations:

(a) Electrode layers, occurring when plasma flows along a flat wall which transitions from insulating to conducting.

(b) Insulator layers, for the reverse transition.

(c) Corner flows, when an electrode has a sharp convex corner which causes the plasma to expand around it to a vacuum.

Cases (a) and (b) are tractable by means of a similarity transformation closely related to those familiar from viscous boundary layer theory. This allows the model to include viscous and other transport effects simultaneously with the magnetic diffusion effect. Exact solutions have been generated and will be presented at the next Electric Propulsion Conference, Case (c) is much more difficult, due to the two-dimensionality. For small corner turning angles, linearization about free-stream is possible, and a complete solution has been obtained by the use of Fourier techniques. This shows the magnetic diffusion smearing the otherwise sharp corner concentration, and also smoothing the current "fan" for distances of many magnetic interaction lengths. This solution will also be presented at the EP conference. Work continues for more realistic large angles, motivated by the need for proper modelling of the anode exit corner flows.

3.4 Arcjet Modeling

In anticipation of the next AFOSR Grant, which focuses in its first year on electrothermal arcjet performance prediction, we have initiated two activities in this area:

(a) The MPD 2-D model of Scott Miller has been expanded by addition of extensive thermochemical and transport submodels for hydrogen (molecular, atomic and ionized), and adapted to axisymmetric geometry. The magnetic field dynamics has been replaced by an elliptic potential equation describing current conservation. We expect this code to become operational very soon, and it will be used for an rigorous analysis of the internal arcjet flows and a prediction of their performance. Extensions to ammonia and other nitrogen - hydrogen mixtures are contemplated.

(b) A new Research Assistant, Miss Atsuko Sakamoto, will start a parallel program in which she will collect and correlate the existing data on arcjects, and will also develop a lower level (finite volume) arcjet model to be used to rapid performance

estimation and correlation. This model will be tuned by comparison to both, the data, and the results of the rigorous 2-D calculations.

3.5 MPD Experiments at Edwards AFB

Doctoral candidate Eric Gaidos will be initiating this Summer a joint experimental program with the Phillips Lab. The goal is the investigation of electrothermal stability of the plasma near full ionization, in an attempt to verify the theory of Refs. 9 and 10. Funding is provided in part by the NSF (Doctoral Fellowship) and in part by the Phillips Laboratory.

References

1. K. Schoemberg and R. Gerwin "Los Alamos Research in Advanced Plasma Thrusters", Presentation to the NASA MPD Thruster Technology Workshop, NASA Headquarters, May 16, 1991.

2. Lin, B.C. and Louis, J.F. Stability of Non-equilibrium MHD Disk Generators". AIAA 26th Aerospace Science Meeting, Jan. 1988.

3. Heimerdinger, D.J., Kilfoyle, D.B. and Martinez-Sanchez, M. "Experimental Characterization of Contoured MPD Thrusters", AIAA-88-3205, 24th JPC, Boston, Ma. 1988.

4. T. Nakayama, K. Toki ad K. Kuriki. "Quantitative Imaging of MPD Flowfields." Paper 88-088, 20th Intnl. Electric Propulsion Conference, Garmisch-Partenkirchen, Germany, 1988.

5. M. Martinez-Sanchez, "The Structure of Self-Field Accelerated Plasma Flows", J. Propulsion and Power, Vol. 7, No. 1, Jan-Feb. 1991, pp 56-65.

6. T.W. Poon, "Local Stability Analysis of the MPD Thruster". Master's Thesis, MIT, Aero/Astro, Sept. 1985.

7. D.J. Heimerdinger and M. Martinez-Sanchez, "Fluid Mechanics in a Magnetoplasmadynamic Thruster", AIAA-88-039, 20th Intnl. Electric Propulsion Conf., Garmisch Partenkirchen, Germany, 1988.

8. D.J. Heimerdinger and M. Martinez-Sanchez, "Design and Performance of an Annular MPD Thruster". To appear in the J. of Propulsion and Power, 1991.

9. E.H. Niewood, J. Preble, D.E. Hastings and M. Martinez-Sanchez. "Electrothermal and Modified Two-Stream Instabilities in MPD Thrusters". AIAA-90-2606, 20th E.P. Conference, Orlando, 1990.

10. J. Preble and M. Martinez-Sanchez. "Onset in MPD Thrusters: A Model of an Electrothermal Instability". Submitted to the AIAA J. of Propulsion and Power (Appended to this Report).

Appendix

Publications during the Reporting Period

Included are the papers

- E.H. Niewood and M. Martinez-Sanchez. "Quasi One-Dimensional Numerical Simulation of MPD Thrusters". Accepted for publication at the AIAA J. of Prop. and Power.

- E. Sheppard and M. Martinez-Sanchez. "Non-Equilibrium Ionization in Plasma Accelerators". AIAA 90-2608, july 1990.

- J. Preble and M. Martinez-Sanchez "Onset in MPD Thrusters: A Model of an Electrothermal Instbility". Submitted to the AIAA J of Prop. and Power.

- S. Miller and M. Martinez-Sanchez. "Viscous and Diffusive Effects in MPD Flows." AIAA 90-2606 July 1990.